JCTC Journal of Chemical Theory and Computation

Sorting Out the Relative Contributions of Electrostatic Polarization, Dispersion, and Hydrogen Bonding to Solvatochromic Shifts on Vertical Electronic Excitation Energies

Aleksandr V. Marenich, Christopher J. Cramer,* and Donald G. Truhlar*

Department of Chemistry and Supercomputing Institute, University of Minnesota, 207 Pleasant Street S.E., Minneapolis, Minnesota 55455-0431

Received May 19, 2010

Abstract: Conventional polarized continuum model calculations of solvatochromic shifts on electronic excitation energies using popular quantum chemical programs (e.g., Gaussian or Turbomole) include the noninertial and inertial bulk-solvent polarization, which will be called electrostatics, but not dispersion interactions and specific effects like hydrogen bonding. For the n→π^* excitation of acetone in several solvents, we estimated the nonelectrostatic contributions in two ways: (i) the vertical excitation model (VEM) of Li et al. (*Int. J. Quantum Chem.* **2000**, *77*, 264), but updated to use TD-DFT corrected linear response with SMD atomic radii, and (ii) in the case of acetone in water, ensemble averaging over supermolecule calculations with up to 12 explicit solvent molecules selected from a molecular dynamics trajectory, with the explicit solvent surrounded by a continuum solvent. The TD-DFT VEM calculations carried out with the M06 density functional for 23 solvents result in a dispersion contribution to the red of 261−356 cm^{-1} and a hydrogen-bonding contribution to the blue of up to 289 cm^{-1}.

1. Introduction

It is well recognized that there are several contributions to solvatochromic effects. These include electric polarization of the solvent and electronic and geometric polarization of the solute, changes in dispersion, exchange repulsion, and cavitation, changes in first-solution-shell specific interactions (such as hydrogen bonding), and charge transfer between solute and solvent. In vertical excitation, it is assumed that vibrational and orientational polarization of the solvent and geometric relaxation of the solute and solvent do not have time to occur (and hence the solvent cavity size does not change if it is assumed to depend only on nuclear positions). Therefore, the following effects remain: (i) electronic polarization of the solvent, (ii) change in dispersion, (iii) change in exchange repulsion, and (iv) charge transfer; furthermore, there are contributions from (v) the interaction of the fixed slow polarization modes of the solvent with the changed electronic structure of the solute and (vi) changes in the energy of hydrogen bonding, because the solvent configuration prior to electronic excitation is equilibrated with the electronic structure of the ground electronic state. We note that the major portion of the hydrogen bonding is electrostatic and is included in (i) and (v); when we refer to hydrogen bonding as a nonelectrostatic phenomenon, we mean the part that is not accounted for in (i) and (v). For example, this could be due to partial covalent character or due to the approximate nature of the treatment of dielectric polarization, including the model used for the solute−solvent boundary assumed in treating (i). In addition, because charge transfer from solute to solvent, that is, (iv), is usually not included explicitly, its especially large contribution to hydrogen bonding must also be considered as a specific first-solvation-shell effect.

Dielectric continuum models of the solvent can include (i) and (v). The primary goal of the present Article is to examine the importance of (ii) and (vi). We shall neglect (iii), which is a short-range effect that is hard to distinguish from the short-range component of (i) and (v). We also neglect explicit consideration of (iv), although it is partly

* Corresponding author e-mail: cramer@umn.edu (C.J.C.); truhlar@umn.edu (D.G.T.).

10.1021/ct100267s
Published on Web 08/25/2010

included in continuum dielectric treatments of (i) because of the empirical nature of the assumed solute−solvent boundary. For convenience, we will introduce the following short-hand names for the effects of interest: (i) fast polarization, (ii) dispersion, (v) slow polarization, and (vi) hydrogen bonding, but the reader should keep in mind that these are just labels for the wordier explanations given in the previous paragraph.

In the present Article, we study the solvatochromic shifts on the vertical n→π^* electronic excitation of acetone in several polar and nonpolar solvents by using two continuum solvation models for calculating the electrostatic component of the shifts as outlined below. Our choice of acetone is motivated by the abundance of experimental[1−9] and theoretical data[10−33] for its n→π^* transition in various solvents, which can be used for comparison to the gas phase. The dipole moment of acetone decreases upon the n→π^* electronic excitation; this, plus the slow response of hydrogen-bonding configurations to vertical excitation, leads to blue solvatochromic shifts in more polar solvents.[28] (A blue shift signifies an increase of the vertical excitation energy in solution relative to the gas phase and indicates that the solute is more favorably solvated in the ground state than in the excited state.) In nonpolar solvents, dispersion and shorter-range repulsion contributions to the corresponding vertical energy can dominate the bulk electrostatic contributions, thereby leading to red (bathochromic) shifts. Indeed, as noted by Rösch and Zerner[12] and earlier by Liptay,[34] the change in solute−solvent dispersion generally leads to red shifts upon vertical excitation. This is also discussed in a previous study from our group.[19]

In a previous study,[19] we presented a treatment (based in part on earlier work[35]) that included the fast and slow polarization, dispersion, and hydrogen bonding. It also included the coupling between the fast and slow polarization but otherwise neglected the coupling of the four identified effects with each other, which is an assumption but probably not a serious one. The previous model[19] treated polarization effects with a two-time formulation of dielectric continuum theory[35] coupled to a configuration interaction model including single excitations (CIS) by intermediate-neglect-of-differential-overlap molecular orbital theory[36,37] (in particular, INDO/S2[38] as incorporated in the ZINDO computer program[39]). Since then, a similar two-time formulation has been coupled[40] to time-dependent density functional theory[41−44] (TD-DFT), which provides a more generally accurate treatment of the electronic states of the solute, and hence potentially a more accurate treatment of the polarization. In the present Article, we re-examine the importance of dispersion and hydrogen bonding using TD-DFT to treat the polarization.

As an alternative to the treatment just described, in which the entire solvent is treated as a continuum, one can consider treating the most strongly coupled solvent molecules explicitly with the rest of the solvent treated as a continuum. We shall also consider this approach here, and we will compare it to the full continuum approach.

2. Theory

2.1. Electrostatics. The accurate theoretical description of solvatochromism, that is, condensed-phase effects on optical absorption and emission spectra, requires a proper account of nonequilibrium solute−solvent interactions, and, therefore, it poses an interesting challenge to theory.[45−49] Whereas adiabatic transition energies correspond to both the initial and the final electronic states of the solute molecule being in equilibrium with a surrounding medium (solvent), vertical transition energies correspond to the final electronic state generated by photon absorption or emission being not equilibrated with the solvent environment. Within the continuum approximation for the polarizable solvent, the treatment of a solute molecule that undergoes an instantaneous change in its charge distribution via an electronic transition caused by photoabsorption or photoemission can be carried out using two time scales for solvent relaxation; these time scales correspond to the fast and slow components for the dynamic polarization response of the solvent.[50,51] The fast polarization component is due to the response of the solvent electrons; this is sometimes called the noninertial polarization. The slow (inertial) response of the solvent is due to its nuclear motions. The fast (electronic) component of the solvent response is in instantaneous equilibrium with the nascent electronic state of the solute, whereas the inertial (nuclear) component is not. This leads to a nonequilibrium free energy that is similar to the nonequilibrium free energy introduced by Marcus in electron-transfer theory.[52] In the present contribution, we consider dielectric medium effects on vertical electronic excitation from an equilibrated ground state to an excited electronic state.

Several dielectric continuum models using self-consistent reaction field (SCRF) theory have been adapted for calculation of vertical electronic transition energies based on two-time-scale response.[19,35,48,49] There are also continuum models that treat multiple time scales using the complex frequency-dependent dielectric permittivity.[53−56] In previous work,[19] our group developed a two-response-time model of vertical excitation energies based on Aguilar et al.'s extension[35] of Marcus's theory of nonequilibrium free energies[52] and on the distributed monopole representation of the solute charge density within the generalized Born approximation.[57−62] A multiconfigurational self-consistent reaction field method that utilizes full multipole expansions of the solute charge field has also been developed.[63] Other methods for calculation of vertical electronic transition energies, for instance, those that use the continuous charge density (without approximating it by distributed point charges or multipoles) within the polarizable continuum model (PCM)[64,65] framework have been reviewed in detail elsewhere.[48] The most recent nonequilibrium version[66,67] of PCM utilizes the state-specific (SS) approach[48] in time-dependent density functional theory (TD-DFT) computations of both absorption and emission energies with analytical PCM/TD-DFT excited state energy gradients.[68] Another recent model exploits a less computationally expensive linear response (LR) approach, which has been corrected with an SS first-order perturbation correction[69] to approximate the SS solvent response within the

integral equation formalism polarizable continuum model (IEF-PCM).[70−73] This method is called corrected linear response (cLR).[69] In addition, Chipman has derived a new formalism for the dielectric continuum treatment of vertical excitations within the surface and volume polarization for electrostatics (SVPE) framework.[74,75] The SVPE method can be approximated through modification of the effective surface polarization without explicit volume polarization by the surface and simulation of volume polarization for electrostatics [SS(V)PE] method,[76,77] which is essentially equivalent to IEF-PCM.[78]

2.2. Specific Effects. The electrostatic treatments described above are labeled bulk electrostatics because the only solvent properties that they use are the bulk static dielectric constant and refractive index. (The square of the latter provides the dielectric constant at optical frequencies.) By invoking the continuum approximation of the solvent, one can eliminate the difficulties associated with the statistical sampling of solvent configuration space in the treatment of bulk electrostatic contributions to solvatochromic shifts. However, continuum models based on bulk electrostatics neglect solvent-structure effects and partial covalency associated with hydrogen bonding, and they do not treat solute−solvent dispersion forces or exchange repulsion of solute and solvent. (Note, however, that the solute−solvent dispersion interaction energy can be partially recovered in the LR approach by means of a term linear in the transition dipole moment between two electronic states of interest.[66,79,80]) The assumption that the electrostatic interactions of the solute and the environment do not depend on the molecular structure of the solvent and that the dielectric response of the medium is isotropic outside the solute cavity can be inaccurate in cases when the solute molecule has strong specific interactions with one or a few solvent molecules in the first solvation shell. In addition, especially in nonpolar solvents, shorter-range (nonbulk) electrostatic effects and nonelectrostatic solute−solvent interactions can be equally or even more important than long-range electrostatic interactions.

In recent years, numerous attempts have been made to incorporate nonbulk electrostatic solvation effects into the treatment of excited electronic states within the continuum approximation. These can be based on atomic surface tensions representing an implicit solvent,[46] or they can include explicit consideration of one or more associated solvent molecules as part of the solute (which is then called a supersolute or supermolecule).[28,46] Using this approach, one can account in part for changes in dispersion, exchange repulsion, or specific solute−solvent interactions (including hydrogen bonding and its associated solute−solvent charge transfer as well as other possible nonbulk-electrostatic and charge transfer effects) upon electronic excitation. However, in explicit models, one must explicitly average over a Boltzmann distribution of solvent orientations, and this rapidly becomes cumbersome as the number of explicit solvent molecules increases. An alternative approach involves addition of special nonelectrostatic corrections to the continuum description, for instance, an exchange repulsion term computed from classical pair potentials.[21]

One model we test here is the vertical electrostatic model (VEM) that was originally based on representing the solute by a set of distributed atomic monopoles within the generalized Born approximation and representing the solvent by its static and optical dielectric constants and augmenting the electrostatics by terms representing dispersion and hydrogen bonding.[19] This model uses intermediate neglect of differential overlap for spectroscopy-parametrization 2 (INDO/S2) and configuration interaction wave functions constructed from single excitations (CIS).[36−38] This model was implemented using the SM5.42 implicit solvation model,[81] and the full vertical excitation model was abbreviated VEM42/INDO/S2 or VEM42. The VEM42 ground-state wave function is evaluated by a closed-shell semiempirical Hartree−Fock self-consistent reaction field (SCRF) calculation with an electrostatic reaction field corresponding to equilibrium solvation. The excited-state wave function is obtained within an iterative configuration interaction calculation including all single excitations with a two-response-time electrostatic reaction field corresponding to equilibrated fast (electronic) solvent response and nonequilibrated Franck−Condon-defined slow (nuclear) solvent response.[19]

Another continuum electrostatic model applied in the present study is the IEF-PCM model based on time-dependent density functional theory (TD-DFT) within the corrected linear response approach of Caricato et al.[69] to treat nonequilibrium solvation effects on vertical excitation spectra. This method is further abbreviated cLR/PCM/TD-DFT or cLR. Here, this kind of calculation is incorporated in the VEM as an improved bulk-electrostatic component that is augmented with contributions accounting for solute−solvent dispersion and hydrogen-bonding effects in the same fashion as in the original VEM model.

We have also studied the effect of making up to 12 water molecules explicit to obtain a better understanding of the way that the first solvation shell affects the magnitude of the solvatochromic shift in aqueous solution. Relevant supermolecular structures were generated from a molecular dynamics trajectory.

In the cLR calculations, we have systematically tested the dependence of calculated solvatochromic shifts on the values of intrinsic atomic Coulomb radii used for construction of the boundary between the solute cavity and the solvent continuum in the bulk electrostatic part of the calculations. In addition to the nine solvents tested in our previous work,[19] we have used the experimental reference data on the $n\rightarrow\pi^*$ absorption of acetone in 23 solvents[9] derived by Renge with the use of a new "band-halving" method for reliable determination of solvent shifts for poorly defined maxima of broad spectral envelopes (Renge corrected inconsistencies in the solvatochromic shifts of acetone existing in older literature for less polar media due to inconsistencies in locating the maxima of broad spectra).[9]

2.3. Detailed Theory. The polarization response of a medium described by the frequency-dependent permittivity $\varepsilon(\omega)$ can be decomposed, within either the Pekar[82] or the Marcus[48] partition, into two terms, fast and slow, as discussed above. The fast polarization component, which is physically due to electronic relaxation, can be described in terms of

the optical dielectric constant ε_{opt} equal to the square of the solvent refractive index, n^2, at an optical frequency (ω_{opt}) at which the slow (mostly orientational) polarization can no longer follow the changes in the field.[45−48] The slow polarization component, which physically requires nuclear motion of the solvent, can be identified by subtracting the fast component from the total polarization, which depends on the solvent static dielectric constant ε. The two partitions differ in that in the Pekar decomposition, the part of the fast polarization that is in equilibrium with nuclear polarization is included in the slow response (along with the polarization due to nuclear movement), but in the Marcus decomposition it is considered as part of the fast response.[48,51] In the limit of linear response, which is assumed, where appropriate, in both the VEM42 and the cLR models, the two decompositions, each used with its corresponding expression for the nonequilibrium free energy, yield identical reaction fields and identical solvatochromic shifts.[51]

If the solvent is represented as a dielectric continuum, the electronic free energy G of the solute molecule in the ground state (G) can be expressed as

$$G_{eq}^{G} = \langle \Psi^{G} | \hat{H}_0 | \Psi^{G} \rangle + \frac{1}{2} \langle \Psi^{G} | V_{fast}^{G} | \Psi^{G} \rangle + \frac{1}{2} \langle \Psi^{G} | V_{slow}^{G} | \Psi^{G} \rangle \quad (1)$$

where $\hat{H}_0$ is the solute electronic Hamiltonian in the gas phase, Ψ^G is the solute electronic wave function in solution (because both the solvent and the solute are mutually polarized, the solute electronic wave function in solution differs from that in the gas phase), and V is the reaction potential induced by the polarization of the dielectric medium. The reaction field is expressed as a sum of its fast and slow components. The subscript "eq" in eq 1 indicates that both the fast and the slow components of the solvent reaction field are equilibrated with the solute charge density for the given electronic state. This equilibration can be achieved routinely through a self-consistent reaction field procedure.[83] Note that the VEM42 model based on the generalized Born approximation constructs the reaction potential V in terms of distributed monopoles (in particular, partial atomic charges), whereas the cLR/IEF-PCM model (or PCM in general) constructs the reaction field in terms of apparent surface charges distributed over the surface of the cavity containing the solute.

For a vertically excited solute molecule in a continuum solvent, the equilibrium free energy of eq 1 is replaced by a more complicated two-response-time nonequilibrium free energy. The detailed equations are given elsewhere[19,35,48,51] for the Marcus decomposition; the more compact expression obtained with the Pekar decomposition is[48]

$$G_{neq}^{E} = \langle \Psi^{E} | \hat{H}_0 | \Psi^{E} \rangle + \frac{1}{2} \langle \Psi^{E} | V_{fast}^{E} | \Psi^{E} \rangle + \langle \Psi^{E} | V_{slow}^{G} | \Psi^{E} \rangle - \frac{1}{2} \langle \Psi^{G} | V_{slow}^{G} | \Psi^{G} \rangle \quad (2)$$

The subscript "neq" indicates a nonequilibrium solvation regime in which only the V_{fast}^{E} component is in equilibrium with the solute charge density, whereas the V_{slow}^{G} component in eq 2 depends on the charge density in the ground state. The calculation of G_{neq}^{E} can be carried out using a two-step procedure: (i) an equilibrium calculation on the ground state (eq 1) to obtain V_{slow}^{G} either in the form of partial atomic charges (SM5.42[84−86] or other[87−89] generalized Born models) or in the form of apparent surface charges (PCM); and (ii) a nonequilibrium calculation on the excited state (eq 2) using the fixed V_{slow}^{G} component while relaxing Ψ^E and V_{fast}^{E}.

The potential V_{fast}^{E} in eq 2 depends on the excited-state wave function of the solute in solution (or the solute's density matrix in solution), and equilibrium between the charge density of the solute excited state and the fast degrees of freedom of the solvent can be obtained through a self-consistent (iterative) procedure using a state-specific approach such as the CIS model in VEM42. These self-consistency iterations are performed for the INDO/S2/CIS model, but for TD-DFT we employ the cLR method, which uses a first-order perturbation correction to obtain an approximation to state-specific solvation in which the slow response of the solvent is in equilibrium with the ground state and the fast response of the solvent is in equilibrium with the specific excited state of interest. This is particularly suitable for use with TD-DFT in which excitation energies are approximated as the poles of frequency-dependent linear response functions of the solute in the ground state, thereby avoiding calculation of the relaxed density matrix of an excited state.

The VEM42 model uses CM2 class IV charges[81,90] obtained from INDO/S2 solute wave functions and the SM5.42 intrinsic Coulomb radii[84,85] to construct molecular cavities in electrostatic calculations. The solvent is represented by its static and dynamic (optical) dielectric constants. All of the VEM42 calculations were carried out using a locally modified version[91] of the ZINDO computer program.[39]

All of the cLR/PCM calculations were performed using time-dependent density functional theory[41−44] (TD-DFT) with the MG3S[92] basis set. The Gaussian 09 program[93] (revision A.02) was employed. The cLR method is also called "StateSpecific", "StateSpecificPerturbation", or "SSPerturbation" in the online manual[94] of Gaussian 09. We employed the Gaussian 09 default settings for nonequilibrium solvation calculations, including the default tessellation algorithm and settings for the cavity definition, but the default intrinsic Coulomb radii were overridden by using the modifysph option to specifically assign values of radii and scaling factors. The tested solvents were defined using additional input keywords, eps and epsinf for static dielectric constant (ε) and for optical dielectric constants ($\varepsilon_{opt} = n^2$), respectively, where n is the solvent refractive index.

Unless noted otherwise, all of the vertical excitation energies of acetone in solution were computed at the molecular geometry of acetone in its ground electronic state optimized in a given solvent with the use of the equilibrium SMD solvation model[95] implemented in Gaussian 09 using the M06-2X[96,97] density functional with the MG3S[92] basis. The corresponding gas-phase vertical excitation energy was computed using the M06-2X/MG3S geometry optimized in the gas phase.

Note that the LR method may include some solvent−solute dispersion,[66,79,80] but an explicit treatment, not used here,

that includes dispersion fully is more complicated.[80] However, in practice the cLR algorithm[69] yields results in reasonable agreement with a method[69] that does not contain any solvent−solute dispersion, and so we proceed under the assumption that the electrostatic calculations do not contain dispersion nor does the bulk electrostatics portion contain specific-solvent effects like hydrogen bonding. The VEM42 and cLR/PCM bulk electrostatic contributions to the solvatochromic shifts were therefore augmented with one-parameter empirical corrections accounting respectively for solute−solvent dispersion and hydrogen-bonding effects, which are the most significant nonelectrostatic contributions. According to ref 19, the total solvatochromic shift is defined as follows:

$$\Delta\omega = \Delta\omega_{EP} + \Delta\omega_{D} + \Delta\omega_{H} \quad (3)$$

where $\Delta\omega_{EP}$ is the electrostatic contribution to the corresponding solvatochromic shift (EP denotes electronic and polarization, i.e., solute electronic energy plus net electric polarization free energy where "net" refers to the accounting, where appropriate, in the derivation of eq 2 for the work done in solvent polarization); $\Delta\omega_{D}$ is the shift due to solvent−solute dispersion; and $\Delta\omega_{H}$ is the shift due to hydrogen bonding. The electrostatic contribution is evaluated as follows:

$$\Delta\omega_{EP} = \omega_{EP}(\text{gas}) - \omega_{EP}(\text{liq}) \quad (4)$$

where ω_{EP}(gas) and ω_{EP}(liq) are the electrostatic contributions to the vertical excitation energies, respectively, in the gas phase and in solution. According to the established sign convention[98] that we use here, a red (bathochromic) shift is called positive (it corresponds to a decrease in frequency and increase in wavelength), and a blue (hypsochromic) shift is called negative (with an increase in frequency and decrease in wavelength). For solvent−solute dispersion ($\Delta\omega_{D}$), we assume a characteristic contribution for a given transition that depends on only the solvent as follows:[1,19]

$$\Delta\omega_{D} = D\frac{n^2 - 1}{2n^2 + 1} \quad (5)$$

where D is a characteristic constant for this particular transition of acetone, and n is the refractive index of the solvent.[19]

The hydrogen-bonding contribution to the n→π* excitation of acetone is likely to be dominated by proton donation from the solvent to the carbonyl oxygen, and this effect should correlate with the proton-donor capability of the solvent.[19] Therefore, we assume

$$\Delta\omega_{H} = H\alpha \quad (6)$$

where H is a model parameter, and α is Abraham's hydrogen-bond acidity parameter[99−102] for a given solvent.

The solvent−solute dispersion contribution (eq 5) and the hydrogen-bonding contribution (eq 6) are added post-SCF, and they do not affect the solute charge distribution.

The model parameters D in eq 5 and H in eq 6 are optimized simultaneously by a least-squares fitting of theoretical $\Delta\omega$ values to the corresponding experimental ones[9] over the set of 23 solvents.

Table 1. Vertical Excitation Energies (ω, cm^{-1}) for the n→π* Transition of Acetone in the Gas Phase[a]

method	ω
CIS/MG3S	42 768
TD-B3LYP/MG3S	36 147
TD-M06/MG3S	36 067
TD-M06-HF/MG3S	28 144
TD-M06-L/MG3S	38 685
TD-M06-2X/MG3S	34 324
INDO/S2	33 055
INDO/S2	33 237[b]
experiments	36 232,[c] 36 100,[d] 35 975[e]
experimental average	36 102

[a] Vertical excitation energies were calculated in the present work at the M06-2X/MG3S geometry optimized in the gas phase unless noted otherwise. [b] Reference 19. [c] Reference 8. [d] Reference 6. [e] Reference 9.

We use the values of solvent dielectric constant ε, refractive index n, and Abraham's hydrogen-bond acidity parameter α presented in the Minnesota Solvent Descriptor Database[103] for all solvents, except for perfluoro-*n*-octane, tetraethoxysilane, *tert*-butyl chloride, and propylene carbonate. For these four solvents, which are not in the database, we use the values of ε and n from ref 9, and we assume that α is zero for these solvents.

3. Results and Discussion

3.1. Treatment with No Explicit Solvent Molecules. First, we performed calculations of the vertical n→π* excitation energies of acetone in the gas phase using TD-DFT with various density functionals (B3LYP,[104−107] M06,[96,97] M06-HF,[97,108] M06-L,[97,109] and M06-2X[96,97]) and the MG3S basis set[92] and using the CIS method[36,110] both with the MG3S basis set[92] and with the semiempirical INDO/S2 model.[19,38] The computational results are compared to the available experimental data in Table 1. The ab initio CIS calculations overestimate the gas-phase excitation energy by ~6670 cm^{-1} on average, whereas the TD-M06-HF method underestimates it by ~7960 cm^{-1}. The B3LYP and M06 density functionals provide the most accurate predictions of the vertical n→π* excitation energies of acetone in the gas phase with respect to the corresponding experimental energies: compare 36 147 (B3LYP), 36 067 (M06), and 35 975−36 232 cm^{-1} (experiment). For this reason, we selected B3LYP and M06 for use in the cLR/PCM/TD-DFT calculations on the vertical n→π* excitations of acetone in solution.

Table 2 shows six types of intrinsic atomic Coulomb radii used in the bulk-electrostatic calculations: Bondi's van der Waals radii,[111] radii optimized for the SM5.42 solvation model,[84,85] radii optimized for the SMD solvation model,[95] united atom topological models UA0[112] and UAHF,[113] and universal force field (UFF) radii.[114] The SM5.42 radii were tested using both the VEM42 and the cLR/PCM methods, whereas the other types were tested only with cLR/PCM. The UFF radii were also tested with the scaling factor of 1.1 and 1.3. Note that the UFF radii scaled by 1.1 are the default radii for excited-state solvation energy calculations in Gaussian 09.

Table 2. Tested Sets of Intrinsic Coulomb Radii (Å)

radii	hydrogen	carbon	oxygen
Bondi[a]	1.2	1.7	1.52
SM5.42[b]	0.91	1.78	1.6
SMD[c]	1.2	1.85	1.52−2.294
UA0[d,e]	n/a	1.925,[f] 2.525[g]	1.75
UAHF[e,h]	n/a	1.68,[f] 1.95[g]	1.59
UFF[e,i]	1.443	1.926	1.75
1.1×UFF[j]	1.5873	2.1186	1.925
1.3×UFF[j]	1.8759	2.5038	2.275

[a] Bondi's values of van der Waals radii.[111] [b] Reference 84. [c] Reference 95. The SMD radius for O is defined as a function of Abraham's hydrogen-bond acidity parameter (α) for a given solvent. It is equal to 1.52 Å for any solvent with $\alpha \geq 0.43$, and it is equal to 2.294 Å for any solvent with $\alpha = 0$. For the solvents with $0 < \alpha < 0.43$, we used the following oxygen radii (in Å): 2.114 (dichloromethane and 1,2-dichloroethane), 2.096 (*cis*-dichloroethylene), 2.222 (acetone), and 2.168 (acetonitrile). [d] The united atom topological model UA0 of the acetone molecule with hydrogen atoms summed into methyl carbon atoms.[112] [e] Values given according to Gaussian 09 output. [f] Carbonyl C atom. [g] Methyl C atom. [h] The united atom topological model UAHF of the acetone molecule with hydrogen atoms summed into methyl carbon atoms.[113] [i] Universal force field (UFF) radii.[114] [j] Scaled UFF radii.

Table 3 shows vertical excitation energies in 23 solvents and the corresponding solvatochromic shifts relative to the gas phase calculated using the cLR/PCM/TD-M06/MG3S electrostatic model with the SMD intrinsic Coulomb radii. Table 4 presents the same quantities calculated with UFF radii scaled by 1.1. The nonelectrostatic contributions ($\Delta\omega_D$ and $\Delta\omega_H$) to the solvatochromic shifts were calculated using the model parameters D (eq 5) and H (eq 6) obtained by a least-squares fitting of $\Delta\omega$ values from eq 3, with theoretical $\Delta\omega_{EP}$ values, to the corresponding experimental values[9] of $\Delta\omega$ over the set of 23 solvents. The optimized values of D and H are given in Table 5 for all tested models. Table 6 shows the corresponding mean signed and mean unsigned errors in $\Delta\omega$ over the set of 23 solvents.

First, we consider only electrostatic contributions $\Delta\omega_{EP}$ to the solvatochromic shifts. Tables 3 and 4 show that the electrostatic contributions ($\Delta\omega_{EP}$) depend on the values of intrinsic Coulomb radii used in electrostatic calculations, and this dependence is strongest with respect to the radius on the carbonyl oxygen. Note that the SMD radius for O is defined as a function of Abraham's hydrogen-bond acidity parameter (α) for a given solvent, whereas the SMD H and C radii and all of the UFF radii are independent of solvent. The SMD radius for O is equal to 1.52 Å for any solvent with $\alpha \geq 0.43$ (in our test set, such solvents are methanol and water), while the corresponding 1.1×UFF radius is 1.925 Å (Table 2). The smaller SMD radius on O leads to a more negative $\Delta\omega_{EP}$, as compared to $\Delta\omega_{EP}$(exp), which is more favorable for acetone in water and less favorable for acetone in methanol. There are five out of 23 solvents with $0 < \alpha < 0.43$ (more specifically, with $0 < \alpha \leq 0.11$), and there are 16 solvents with $\alpha = 0$. For these 21 solvents, the SMD oxygen radius ranges from 2.096 (for *cis*-dichloroethylene with $\alpha = 0.11$) to 2.294 Å (for *n*-pentane and others with $\alpha = 0$), and the SMD electrostatic contributions $\Delta\omega_{EP}$ to the corresponding solvatochromic shifts are similar to those obtained using the 1.1×UFF radii.

In general, the error associated with comparing the $\Delta\omega_{EP}$ values directly to experiment, averaged over 23 solvents (Table 6) decreases if a higher scaling factor for intrinsic Coulomb radii is used (e.g., compare the results for 1.3×UFF to those for UFF). However, the scaling of Coulomb radii can lead to unphysical values of the radii, and the scaling alone cannot provide a reliable method because reliable calculations must take into account not only bulk electrostatics (that is, long-range electrostatic polarization effects and the part of the short-range electrostatic effect that is adequately modeled with bulk parameters and the chosen radii) but also nonelectrostatic effects, the most significant of which are solute−solvent dispersion and hydrogen-bonding effects. On the other hand, there is no unique way to separate the bulk electrostatic contribution to the free energy of solvation from the remainder.[88,89,115,116] Indeed, Table 5 indicates the strong dependence of optimized dispersion and hydrogen-bonding model parameters on the choice of intrinsic Coulomb radii used in bulk-electrostatic calculations, but the two-parameter model (with parameters D and H) allows one to correct the $\Delta\omega_{EP}$ contributions in the right direction relative to experiment over all sets of radii and tested solvents with only one exception, dioxane in which case the computed value of $\Delta\omega_{EP}$ (for instance, −231 with the SMD radii and −246 cm^{-1} with the 1.1×UFF radii, Tables 3 and 4) appears overly "red" with respect to the corresponding experimental value[9] ($\Delta\omega = -305$ cm^{-1}) because the values of the O radius in our calculations are apparently too large for dioxane, resulting in the ground electronic state of the acetone molecule in dioxane being undersolvated.

The models using the UA0 radii (in which case one assigns types to atoms and treats certain groups consisting of an atom and its covalently attached hydrogens as a united atom) are quite accurate as well. However, sometimes it is preferable to use a model that does not require the user to assign molecular-mechanics types to an atom or group, and such assignments may be ambiguous if the hybridization changes upon electronic excitation.

Table 6 indicates that the errors in VEM42/INDO/S2 calculations are smaller than those in most of the PCM/TD-DFT calculations. However, the semiempirical VEM42/INDO/S2 method is likely to underestimate the $\Delta\omega_{EP}$ contributions, especially in polar solvents, and this results in the hydrogen-bonding contribution being overestimated by eq 6. Note that INDO/S2 gives an error of ~3000 cm^{-1} (Table 1) for predicting the gas-phase vertical excitation energy, which is not competitive with good density functional calculations.[117]

Table 5 indicates that the sign of the H parameter is negative, and it signifies that hydrogen-bonding contributes in the direction of the shift being blue, in agreement with conclusions in earlier work.[19] The sign of the D parameter is positive, meaning that solute−solvent dispersion contributes toward a red shift. Indeed, as noted in the introduction, the change in solute−solvent dispersion generally leads to red shifts. One of the tested models (Table 5) results in a negative value of D. However, this model is just a null test that does not include any electrostatics (the $\Delta\omega_{EP}$ contribu-

Table 3. Vertical Excitation Energies (ω, cm^{-1}) and Solvatochromic Shifts ($\Delta\omega$, cm^{-1}) for the n→π^* Transition of Acetone in 23 Solvents Calculated Using the cLR/PCM/TD-M06/MG3S Electrostatic Model with the SMD Coulomb Radii[a]

solvent				exp		theory[b]					deviation
name	ε	n	α	ω	$\Delta\omega$	ω_{EP}	$\Delta\omega_{EP}$	$\Delta\omega_D$	$\Delta\omega_H$	$\Delta\omega$	$\Delta\Delta\omega$
gas phase	1	1	0	35 975		36 067					
perfluoro-*n*-octane	1.7	1.3	0	36 130	−155	36 230	−164	261	0	97	252
n-pentane	1.8371	1.3575	0	35 950	25	36 243	−177	298	0	121	96
n-hexane	1.8819	1.3749	0	35 940	35	36 249	−182	308	0	126	91
n-heptane	1.9113	1.3878	0	35 935	40	36 253	−186	316	0	130	90
n-decane	1.9846	1.4102	0	35 920	55	36 263	−197	329	0	132	77
n-hexadecane	2.0402	1.4345	0	35 950	25	36 269	−202	342	0	140	115
carbon tetrachloride	2.228	1.4601	0	35 695	280	36 296	−229	356	0	127	−153
dioxane	2.2099	1.4224	0	36 280	−305	36 297	−231	336	0	105	410
tetraethoxysilane	2.5	1.382	0	36 104	−129	36 364	−298	312	0	15	144
diethyl ether	4.24	1.3526	0	36 155	−180	36 536	−469	295	0	−175	5
methyl acetate	6.8615	1.3614	0	36 308	−333	36 652	−586	300	0	−285	48
tetrahydrofuran	7.4257	1.405	0	36 272	−297	36 655	−589	326	0	−263	34
sec-butyl chloride	8.393	1.3971	0	36 132	−157	36 683	−616	321	0	−295	−138
dichloromethane	8.93	1.4242	0.1	36 300	−325	36 775	−708	337	−35	−407	−82
cis-dichloroethylene	9.2	1.449	0.11	36 170	−195	36 783	−716	350	−39	−405	−210
tert-butyl chloride	9.663	1.385	0	36 120	−145	36 713	−646	314	0	−332	−187
1,2-dichloroethane	10.125	1.4448	0.1	36 280	−305	36 792	−725	348	−35	−413	−108
acetone, neat	20.493	1.3588	0.04	36 373	−398	36 844	−778	299	−14	−493	−95
acetonitrile	35.688	1.3442	0.07	36 440	−465	36 925	−858	289	−25	−593	−128
dimethyl sulfoxide	46.826	1.417	0	36 350	−375	36 834	−767	333	0	−434	−59
propylene carbonate	62.93	1.421	0	36 393	−418	36 848	−782	335	0	−447	−29
methanol	32.613	1.3288	0.43	36 916	−941	37 535	−1,469	280	−152	−1,341	−400
water	78.3553	1.333	0.82	37 760	−1,785	37 569	−1,502	282	−289	−1,509	276

[a] Solvents are sorted as in ref 9. Vertical excitation energies in the gas phase and in solution and solvatochromic shifts with respect to the gas phase are calculated over the test set of 23 solvents. Solvent descriptors are dielectric constant (ε), refractive index (n), and Abraham's hydrogen-bond acidity parameter (α). Theoretical solvatochromic shifts ($\Delta\omega$) are expressed in terms of the corresponding electronic-polarization (EP), dispersion (D), and hydrogen-bonding (H) components (see eqs 3−6). The $\Delta\Delta\omega$ values refer to the difference between $\Delta\omega$(theory) and $\Delta\omega$(experiment). [b] The PCM/TD-M06 vertical excitation energies in solution were calculated using the M06-2X/MG3S molecular geometries of acetone optimized in solution by the SMD implicit solvation model, whereas the corresponding gas-phase vertical excitation energy of acetone was calculated at the M06-2X/MG3S geometry optimized in the gas phase.

Table 4. Vertical Excitation Energies (ω, cm^{-1}) and Solvatochromic Shifts ($\Delta\omega$, cm^{-1}) for the n→π^* Transition of Acetone in 23 Solvents Calculated Using the cLR/PCM/TD-M06/MG3S Electrostatic Model with the UFF Coulomb Radii Scaled by the Factor of 1.1[a]

solvent				exp		theory[a]					deviation
name	ε	n	α	ω	$\Delta\omega$	ω_{EP}	$\Delta\omega_{EP}$	$\Delta\omega_D$	$\Delta\omega_H$	$\Delta\omega$	$\Delta\Delta\omega$
gas phase	1	1	0	35 975		36 067					
perfluoro-*n*-octane	1.7	1.3	0	36 130	−155	36 239	−173	283	0	111	266
n-pentane	1.8371	1.3575	0	35 950	25	36 252	−186	323	0	138	113
n-hexane	1.8819	1.3749	0	35 940	35	36 259	−193	335	0	142	107
n-heptane	1.9113	1.3878	0	35 935	40	36 263	−196	343	0	147	107
n-decane	1.9846	1.4102	0	35 920	55	36 275	−208	357	0	149	94
n-hexadecane	2.0402	1.4345	0	35 950	25	36 281	−215	372	0	157	132
carbon tetrachloride	2.228	1.4601	0	35 695	280	36 310	−244	387	0	143	−137
dioxane	2.2099	1.4224	0	36 280	−305	36 313	−246	364	0	118	423
tetraethoxysilane	2.5	1.382	0	36 104	−129	36 384	−318	339	0	22	151
diethyl ether	4.24	1.3526	0	36 155	−180	36 573	−507	320	0	−186	−6
methyl acetate	6.8615	1.3614	0	36 308	−333	36 699	−632	326	0	−306	27
tetrahydrofuran	7.4257	1.405	0	36 272	−297	36 701	−635	354	0	−281	16
sec-butyl chloride	8.393	1.3971	0	36 132	−157	36 731	−665	349	0	−316	−159
dichloromethane	8.93	1.4242	0.1	36 300	−325	36 697	−630	366	−169	−433	−108
cis-dichloroethylene	9.2	1.449	0.11	36 170	−195	36 691	−624	380	−186	−430	−235
tert-butyl chloride	9.663	1.385	0	36 120	−145	36 763	−696	341	0	−355	−210
1,2-dichloroethane	10.125	1.4448	0.1	36 280	−305	36 712	−645	378	−169	−436	−131
acetone, neat	20.493	1.3588	0.04	36 373	−398	36 844	−778	324	−68	−521	−123
acetonitrile	35.688	1.3442	0.07	36 440	−465	36 878	−811	314	−118	−615	−150
dimethyl sulfoxide	46.826	1.417	0	36 350	−375	36 891	−824	361	0	−463	−88
propylene carbonate	62.93	1.421	0	36 393	−418	36 905	−838	364	0	−474	−56
methanol	32.613	1.3288	0.43	36 916	−941	36 663	−596	304	−727	−1,019	−78
water	78.3553	1.333	0.82	37 760	−1785	36 653	−586	307	−1,386	−1,665	120

[a] See footnotes of Table 3.

tions are assumed to be zero), and the exception merely proves that a separate (unbalanced) treatment of bulk-electrostatic and nonelectrostatic contributions may lead to spurious results.

The SMD intrinsic Coulomb radii lead to good agreement with experiment, whereas the UFF radii need to be increased to provide good accuracy. Comparison of the $\Delta\omega_{EP}$, $\Delta\omega_D$, and $\Delta\omega_H$ components in Tables 3 and 4 indicates that the

Table 5. Model Parameters for Dispersion (*D*) and Hydrogen-Bonding (*H*) Components (cm^{-1}) Optimized over Reference Data in 23 Solvents[a]

electrostatic model	radii[b]	*D*	*H*
no electrostatics[c]	n/a	−685	−2007
PCM/TD-B3LYP	Bondi	4351	−837
PCM/TD-B3LYP	SM5.42	4516	−861
PCM/TD-B3LYP	SMD	1487	−514
PCM/TD-B3LYP	UA0	1757	−1658
PCM/TD-B3LYP	UAHF	4288	−901
PCM/TD-B3LYP	UFF	2525	−1432
PCM/TD-B3LYP	1.1×UFF	1557	−1749
PCM/TD-B3LYP	1.3×UFF	362	−2111
PCM/TD-M06	Bondi	4795	−721
PCM/TD-M06	SM5.42	4909	−759
PCM/TD-M06	SMD	1655	−353
PCM/TD-M06	UA0	2035	−1588
PCM/TD-M06	UAHF	4686	−797
PCM/TD-M06	UFF	2835	−1353
PCM/TD-M06	1.1×UFF	1798	−1690
PCM/TD-M06	1.3×UFF	520	−2076
VEM42/INDO/S2	SM5.42	1589	−1646
VEM42/INDO/S2[d]	SM5.42	3448	−1614

[a] The notation PCM refers to the cLR/PCM/TD-DFT/MG3S calculations. Unless noted otherwise, two model parameters (*D* and *H*) describing dispersion and hydrogen-bonding contributions to the solvatochromic shift for the n→π* transition of acetone were optimized using eqs 3−6 over 23 experimental reference data and the corresponding electrostatic (EP) contributions calculated using the given combinations of vertical electrostatic models and Coulomb radii. Vertical excitation energies in solution were calculated using the M06-2X/MG3S molecular geometries of acetone optimized in solution by the SMD implicit solvation model, whereas the corresponding gas-phase vertical excitation energy of acetone was calculated at the M06-2X/MG3S geometry optimized in the gas phase. [b] See footnotes of Table 2. [c] The EP contribution is neglected. [d] Taken from ref 19, where the experimental data set used for parametrization was older and smaller than that used here.

values of $\Delta\omega_D$ calculated using the 1.1×UFF radii are close to the corresponding values calculated using the SMD radii. Indeed, the dispersion contribution in 23 solvents varies between 261 and 356 cm^{-1} when the SMD radii are used and between 283 and 387 cm^{-1} when the 1.1×UFF radii are used. However, the absolute values of $\Delta\omega_H$ in the SMD case are much smaller than those calculated using the 1.1×UFF radii. Thus, we assume that in the SMD case most of the hydrogen-bonding effect on solvatochromic shifts in solvents that exert such an effect (i.e., in solvents with nonzero Abraham's hydrogen-bond acidity parameter α) can be implicitly accounted for through the bulk-electrostatic contribution $\Delta\omega_{EP}$, in part due to the dependence of the SMD Coulomb radius of the oxygen atom on the value of α. Note that the magnitude of $\Delta\omega_{EP}$ is more sensitive to the O radius value than to the values of the Coulomb radii on C and H, which are independent of solvent in the present work. Note also that the variation in the O radius was not adopted especially for purposes of the present calculations, but has always been part of the SMD solvation model[95] where it is required to obtain accurate equilibrium free energies of solvation for ground-state ions in nonaqueous solutions. The absolute values of the *H* parameter obtained using the SMD radii for bulk electrostatics are relatively small, and they are 3−5 times smaller than those optimized within the 1.1×UFF model (Table 5). Upon neglect of the $\Delta\omega_H$ contribution (*H* = 0), the RMSE over 23 solvents increases only slightly if the SMD radii are used (for instance, in the case of TD-M06 calculations from 175 to 189 cm^{-1}), but the error increase is more significant (from 158 to 369 cm^{-1}) if the 1.1×UFF radii are used. We conclude that the use of UFF radii scaled by 1.1 (Gaussian 09 default radii) for calculation of the vertical n→π* excitation energy of acetone in water (and, perhaps, in other cases) requires the $\Delta\omega_H$ correction for the bulk-electrostatic (electron-polarization) component because the bulk-electrostatic contribution is underestimated when the 1.1×UFF radii are used. We note, however, that our assessment at this point is specific to the case we are studying here, and by extension perhaps carbonyls in general, but will need to be further investigated for other chromophores.

Table 6 also shows the errors in $\Delta\omega$ using the gas-phase molecular geometry of acetone in vertical excitation energy calculations in solution instead of geometries optimized for the ground state in the particular solvent using the SMD[95] solvation model. Note that the use of solvent-specific geometries of acetone is the default in the present study, while in the previous study[19] only a gas-phase geometry was used. Optimizing the molecular geometry of acetone in solution leads to a substantial increase of the C−O distance in more polar media, which, in turn, leads to a substantial decrease of the $\Delta\omega_{EP}$ contribution to the corresponding solvatochromic shift. For example, the M06-2X/MG3S optimization yields $R_e(CO) = 1.204$ Å in the gas phase and $R_e(CO) = 1.218$ Å in water. The corresponding TD-M06/MG3S gas-phase excitation energy at the gas-phase geometry is 36 067 cm^{-1}, the cLR/PCM/TD-M06/MG3S (with the SMD Coulomb radii) excitation energy of acetone in water at the water-specific optimized geometry is 37 569 cm^{-1}, and the corresponding EP contribution to the shift is $\Delta\omega_{EP} = -1502$ cm^{-1}. Using the TD-M06/MG3S gas-phase geometry in the cLR/PCM/TD-M06/MG3S calculation leads to an excitation energy of acetone in water equal to −38 026 cm^{-1}, with the corresponding EP contribution equal to $\Delta\omega_{EP} = -1959$ cm^{-1}. This trend agrees with the results of previous calculations.[22,28] Table 6 shows that using the gas-phase geometry decreases the accuracy of the theoretical values of $\Delta\omega$ across all of the electrostatic models tested in the present work.

Table 7 presents partial atomic charges and dipole moments for the ground and for the first excited electronic state of the acetone molecule in the gas phase and in *n*-hexane and water. The partial atomic charges were calculated using the Merz−Singh−Kollman electrostatic potential fitting method[118,119] implemented in Gaussian 09.[93] The dipole moment of the acetone molecule in solution increases in comparison with the gas-phase dipole moment in both the ground and the first excited electronic states, and the polarity of the acetone molecule increases with the polarity of the solvent (as seen by comparing the results for *n*-hexane and water). The ground-state dipole moment of the acetone molecule is higher than the excited-state dipole moment, and the difference is larger for more polar solvents because the acetone molecule is more favorably solvated in its ground state than in the nascent excited state. The trends in the partial atomic charges on the carbon and oxygen atoms of the

Table 6. Errors in Vertical Excitation Energy Solvatochromic Shifts (cm^{-1}) for the n→π* Transition of Acetone in 23 Solvents[a,b]

		gas-phase geometry[c]				liquid-phase geometry[d]			
		EP		EPDH		EP		EPDH	
electrostatic model	radii[e]	MSE	MUE	MSE	MUE	MSE	MUE	MSE	MUE
no electrostatics[f]	n/a	280[g]	320[g]	4	137	280[g]	320[g]	4	137
PCM/TD-B3LYP	Bondi	−963	963	2	397	−767	786	2	352
PCM/TD-B3LYP	SM5.42	−982	982	2	381	−797	815	2	341
PCM/TD-B3LYP	SMD	−461	461	2	172	−244	289	2	130
PCM/TD-B3LYP	UA0	−435	491	3	185	−212	350	3	138
PCM/TD-B3LYP	UAHF	−944	944	2	376	−751	774	2	333
PCM/TD-B3LYP	UFF	−590	624	2	240	−375	460	3	190
PCM/TD-B3LYP	1.1×UFF	−393	456	3	165	−167	322	3	119
PCM/TD-B3LYP	1.3×UFF	−152	280	3	97	88	203	4	93
PCM/TD-M06	Bondi	−1053	1053	2	430	−861	867	2	387
PCM/TD-M06	SM5.42	−1061	1061	2	409	−880	886	2	371
PCM/TD-M06	SMD	−504	504	2	184	−288	319	2	140
PCM/TD-M06	UA0	−492	540	3	203	−270	390	3	154
PCM/TD-M06	UAHF	−1025	1025	2	406	−834	846	2	364
PCM/TD-M06	UFF	−653	678	2	263	−440	510	3	211
PCM/TD-M06	1.1×UFF	−443	499	3	181	−217	357	3	132
PCM/TD-M06	1.3×UFF	−185	303	3	103	55	197	4	88
VEM42/INDO/S2	SM5.42	−264	358	3	112	−181	318	3	100

[a] Mean signed (MSE) and mean unsigned (MUE) errors refer to the difference between theoretical and experimental solvatochromic shifts. EPDH denotes electronic (E), polarization (P), dispersion (D), and hydrogen-bonding (H) contributions to the solvatochromic shift. The EP contributions were calculated using the given combinations of vertical electrostatic models and Coulomb radii, whereas the corresponding DH contributions were either neglected (the EP column) or determined within the two-parameter model (eqs 3−6). [b] The corresponding experimental energies include 23 reference data from ref 9. [c] Vertical excitation energies in solution and in the gas phase were calculated using the ground-state gas-phase geometry optimized at the M06-2X/MG3S level of theory. [d] Vertical excitation energies in solution were calculated using the M06-2X/MG3S molecular geometries of acetone optimized in solution by the SMD implicit solvation model, whereas the corresponding gas-phase vertical excitation energy of acetone was calculated at the M06-2X/MG3S geometry optimized in the gas phase. The corresponding model parameters *D* and *H* used to calculate nonelectrostatic (DH) contributions are given in Table 5. [e] See footnotes of Table 2. [f] The EP contribution is neglected. [g] The solvatochromic shift (EPDH) is assumed to be zero.

carbonyl group and in the magnitudes of the dipole moment of the acetone molecule in *n*-hexane and water obtained using the SMD Coulomb radii are qualitatively similar to the trends in the corresponding values obtained using the UFF radii scaled by 1.1 (Table 7). However, the use of the SMD Coulomb radii results in a higher dipole moment in the more polar solvent. It is difficult to further quantify the accuracy of either the SMD or the 1.1×UFF radii for predicting the dipole moment in solution because of the absence of experimental liquid-phase dipole moments. Note that experimental dipole moments are readily available for gas-phase molecules[120] but not for molecules in solution, where the dipole moment is not even uniquely defined, irrespective of the electronic state.

Table 8 contains predicted solvatochromic shifts on the vertical n→π* excitation transition of acetone for 18 common solvents that were not included in the training set of 23 solvents.[9] These solvents are a subset of the Minnesota Solvent Descriptor Database.[103] The Supporting Information gives predictions of solvatochromic shifts for all 178 solvents of the database.

3.2. Mixed Discrete-Continuum Models. We have studied the effect of adding up to 12 water molecules explicitly to the acetone molecule with the solute and explicit water molecules treated as a supermolecule immersed in an aqueous continuum. The clusters were constructed using 20 random acetone−water configurations obtained from a molecular dynamics (MD) simulation. The MD simulation was performed with the Macromodel utility[121] in the Maestro Version 8.5 computational package[122] using a cubic box of 37.3 × 37.3 × 37.3 $Å^3$ containing 1733 water molecules and one rigid acetone molecule (fixed at the aqueous-phase geometry optimized at the SMD/M06-2X/MG3S level of theory), the OPLS_2005 force field[123] with the force-field-defined electrostatic treatment and charges, a temperature of 300 K, a time step of 1.5 fs, and an equilibration time of 200 ps. The simulation was carried out for 2 ns, and configurations were written every 100 ps. The OPLS_2005 force field[123] is an enhanced version of the OPLS all-atom force field of Jorgensen et al.[124] For each of the 20 configurations, we defined a supermolecular cluster by retaining the 12 water molecules closest to the oxygen atom in the acetone molecule (as determined by the distance from the carbonyl oxygen to the nearest hydrogen of the water molecule). We also defined smaller clusters as subsets of these in which we retained only the 1, 2, 5, 8, or 10 closest water molecules.

Table 9 shows values of the vertical excitation energy (ω) and solvatochromic shift ($\Delta\omega$) for the n→π* transition of acetone in water estimated by averaging over the corresponding energies calculated for the 20 acetone−water clusters including *n* water molecules explicitly (where *n* varies between 1 and 12) and treating the rest within the continuum approximation. All of the energies in Table 9 nominally contain only bulk-electrostatic (electron-polarization) effects with $H = D = 0$, but it should be noticed that hydrogen bonding and dispersion-like attractive noncovalent interactions between acetone and the explicit water molecules are included by treating acetone and the explicit waters with the M06 density functional.

Table 7. Partial Atomic Charges (au) and Dipole Moments (debye) Calculated for the Acetone Molecule in the Ground and First Excited Electronic States[a]

	SMD radii[b]		1.1×UFF radii[b]		gas[c]	
method	ground	excited	ground	excited	ground	excited
Solvent: *n*-Hexane						
q(C)	0.80	0.43	0.80	0.43	0.79	0.43
q(O)	−0.59	−0.34	−0.59	−0.34	−0.56	−0.32
μ_q	3.45	2.00	3.45	1.99	3.14	1.78
μ_ρ	3.47	2.02	3.46	2.01	3.15	1.80
Solvent: Water						
q(C)	0.86	0.46	0.81	0.44	0.78	0.43
q(O)	−0.71	−0.40	−0.65	−0.37	−0.57	−0.32
μ_q	4.67	2.72	4.16	2.37	3.23	1.78
μ_ρ	4.70	2.76	4.19	2.40	3.24	1.78

[a] The notations q(C) and q(O) refer to the partial atomic charges on the carbon and the oxygen atom in the carbonyl group, respectively. The notations μ_q and μ_ρ refer to the dipole moment calculated based on the partial atomic charges and the quantum-mechanical electronic density, respectively. The partial atomic charges were obtained with the Merz−Singh−Kollman electrostatic potential fitting method.[118,119] The ground- and excited-state electronic densities were calculated at the TD-M06/MG3S level of theory. The excited-state electronic density of the acetone molecule in solution was calculated using the ground-state reaction field. [b] Calculated using the polarizable continuum solvent approximation and the corresponding Coulomb radii at the SMD/M06-2X/MG3S ground-state geometry of the acetone molecule optimized in *n*-hexane and water. [c] Calculated in the gas phase at the SMD/M06-2X/MG3S ground-state geometry of the acetone molecule optimized in *n*-hexane and water; the calculation at the corresponding gas-phase optimized geometry was also performed: q(C) = 0.79, q(O) = −0.56, μ_q = 3.12, μ_ρ = 3.13 (ground state), and q(C) = 0.43, q(O) = −0.32, μ_q = 1.79, μ_ρ = 1.80 (excited state). For comparison, the experimental gas-phase value of μ is 2.88 ± 0.03 debye (ground state).[120]

Table 8. Predicted Solvatochromic Shifts ($\Delta\omega$, cm^{-1}) for the n→π^* Transition of Acetone in 18 Common Organic Solvents[a]

name	ε	n	α	$\Delta\omega$
acetic acid	6.2528	1.3720	0.61	−934
benzene	2.2706	1.5011	0	147
carbon disulfide	2.6105	1.6319	0	177
chloroform	4.7113	1.4459	0.15	−292
cyclohexane	2.0165	1.4266	0	136
diethylamine	3.5766	1.3864	0.08	−171
diiodomethane	5.3200	1.7425	0.05	−26
N,N-dimethylformamide	37.2190	1.4305	0	−417
ethanol	24.852	1.3611	0.37	−1135
ethyl acetate	5.9867	1.3723	0	−250
methylcyclohexane	2.0240	1.4231	0	132
4-methyl-2-pentanone	12.8870	1.3962	0	−360
2-methyl-1-propanol	16.7770	1.3955	0.37	−1034
1-octanol	9.8629	1.4295	0.37	−876
pyridine	12.9780	1.5095	0	−271
tetrachloroethene	2.2680	1.5053	0	148
toluene	2.3741	1.4961	0	126
2,2,2-trifluoroethanol	26.7260	1.2907	0.57	−1414

[a] Solvatochromic shifts are calculated using the cLR/PCM/TD-M06/MG3S method and SMD Coulomb radii for vertical bulk-electrostatic energies augmented with the corresponding solute−solvent dispersion and hydrogen-bonding contributions. Solvent descriptors are dielectric constant (ε), refractive index (n), and Abraham's hydrogen-bond acidity parameter (α).[103]

Figure 1 shows an example of the cluster containing five explicit water molecules. The value of $\Delta\omega$ averaged over 20 clusters (with n water molecules in each) depends on n,

Table 9. Vertical Excitation Energies (ω, cm^{-1}) and Solvatochromic Shifts ($\Delta\omega$, cm^{-1}) for the n→π^* Transition of Acetone in Water Calculated Using Acetone−Water Clusters and Implicit Solvent Models[a]

method	radii	n	ω	$\Delta\omega$	SD
gas					
TD-B3LYP[b]			36 147		
TD-M06[b]			36 067		
INDO/S2[b]			33 055		
experiment (ref 9)			35 975		
continuum[c]					
PCM/TD-B3LYP	SMD	0	37 510	−1363	
PCM/TD-B3LYP	SMD	12	37 631	−1484	479
PCM/TD-M06	SMD	0	37 569	−1502	
PCM/TD-M06	SMD	1	37 796	−1730	313
PCM/TD-M06	SMD	2	37 863	−1797	452
PCM/TD-M06	SMD	5	37 788	−1721	466
PCM/TD-M06	SMD	8	37 769	−1703	463
PCM/TD-M06	SMD	10	37 763	−1697	492
PCM/TD-M06	SMD	12	37 742	−1675	474
PCM/TD-M06[d]	SMD	1	38 373	−2307	
PCM/TD-M06[d]	SMD	2	39 003	−2936	
PCM/TD-M06	1.1×UFF	0	36 653	−586	
PCM/TD-M06	1.1×UFF	1	37 089	−1023	406
PCM/TD-M06	1.1×UFF	12	37 212	−1146	675
VEM42/INDO/S2	SM5.42	0	33 661	−606	
VEM42/INDO/S2	SM5.42	12	33 222	−167	256
VEM42/INDO/S2[e]	SM5.42	12	33 262	−207	237
experiment (ref 9)			37 760	−1785	

[a] The MG3S basis set was used in all TD-DFT calculations. [b] The vertical excitation energy of bare acetone in the gas phase was calculated with a given method at the M06-2X/MG3S optimized gas-phase geometry. [c] Vertical excitation energies of acetone−water clusters (ω) containing n water molecules and that of bare acetone (n = 0) in water were calculated using given implicit solvation models and Coulomb radii. The values of ω were averaged over 20 random acetone−water configurations obtained from an MD simulation unless noted otherwise. They contain no dispersion and hydrogen-bonding corrections, and they nominally correspond to ω_{EP}. The $\Delta\omega$ values were calculated relative to the gas-phase vertical excitation energy of bare acetone. SD stands for standard deviation. [d] Not an average, but a single-point energy calculation with the SMD/M06-2X/MG3S optimized liquid-phase geometry of an acetone−water cluster corresponding to the global minimum (Figure 2). [e] Calculated over 100 random acetone−water configurations obtained from an MD simulation.

but this dependence is small for $n \geq 5$. The averaged theoretical values of $\Delta\omega$ are in good agreement with the experimental value[9] (−1785 cm^{-1}) when we use the SMD intrinsic Coulomb radii: −1675 cm^{-1} (M06, n = 12). The use of the 1.1×UFF radii instead leads to an underestimated blue shift (−1146 cm^{-1}) in these calculations (M06, n = 12). The least accurate model in these calculations is VEM42/INDO/S2, which severely underestimates the blue shift (−167 cm^{-1}) with respect to experiment, apparently due to an underestimate of the hydrogen bonding in the acetone−water clusters at the INDO/S2 level.

Table 9 also shows a result for the VEM42/INDO/S2 model when we average over all 100 acetone−water clusters. The absolute value of ω changes by 40 cm^{-1} in comparison with the value of ω averaged over only 20 clusters. Although the averaging over larger numbers of MD snapshots can lead to a more precise prediction of the solvatochromic shift for a given model chemistry, we have chosen to use only 20 acetone−water clusters in most of the calculations because

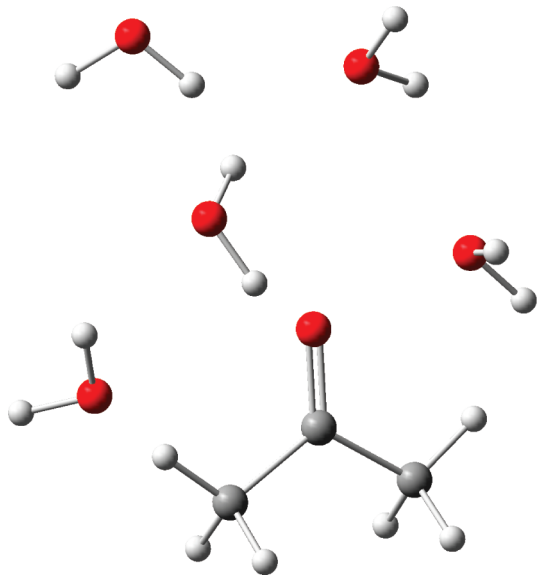

Figure 1. An example of the solute−solvent cluster containing five explicit water molecules. Hydrogen atoms are white, carbon is gray, and oxygen is red.

this choice provides for a reasonable balance of computational time-saving and small sampling error.

The values of ω and $\Delta\omega$ averaged over the 20 MD clusters in aqueous solution are also compared in Table 9 to those calculated for a single solute−solvent cluster with one or two water molecules at the ground-state molecular geometry optimized in solution by the SMD/M06-2X/MG3S method (Figure 2). This approach with a single solute−solvent cluster, which is widely used in the literature, overestimates the blue shift by 522−1151 cm^{-1} with respect to the experimental value,[9] and in the present study it is substantially less accurate than the method that considers a dynamically generated distribution of solvent orientations.

3.3. Comparison with Other Models. Solvatochromic shifts on the vertical n→π* excitation of acetone have been the subject of numerous theoretical studies.[11−33,75] Here, we discuss results of several recent calculations of the vertical n→π* excitation energy of acetone in water.[21,22,28,75] The results of these previous studies[21,22,28,75] are presented in Table 10, where they are compared to selected results obtained in the present work.

Cossi and Barone[21] employed the conductor-like version of PCM (C-PCM) that incorporated a computation of the final (excited) state at the CASSCF/6-31G(d) level. Quantum-mechanical terms for solute−solvent dispersion and repulsion interactions were included in the solute Hamiltonian to take into account the nonelectrostatic contributions to solvatochromic shifts, assuming no contribution from cavitation effects.[21] They obtained the following dispersion−repulsion contributions to solvatochromic shifts:[21] 606, 409, 397, and 378 cm^{-1} in cyclohexane, dichloromethane, ethanol, and water, respectively (within the sign convention adopted in the present work). Except for cyclohexane, these numbers are in qualitative agreement with the values of $\Delta\omega_D$ predicted in the present work using the cLR/PCM/TD-M06/MG3S method with the SMD Coulomb radii, 338, 337, 300, and 282 cm^{-1} in the same four solvents, respectively. Aquilante et al.[22] carried out a TD-DFT computation of the acetone ultraviolet spectrum in aqueous solution using the PBE0 density functional and mixed discrete/continuum models. The authors noticed that the attachment of two explicit water molecules to the carbonyl oxygen of the acetone molecule (with the cluster being optimized) led to an overly blue solvatochromic shift predicted by PCM, and the computed shifts were sensitive to the orientation of the solvent molecules around the carbonyl group.[22] These observations by Aquilante et al.[22] are confirmed in the present study with M06.

Aidas et al.[28] applied the combined linear response coupled cluster/molecular mechanics (CC/MM) scheme including mutual polarization effects in the coupling Hamiltonian to the study of the vertical n→π* excitation energy of acetone in water, by averaging over 800 solute−solvent configurations obtained from a molecular dynamics simulation. A spherical cutoff radius of 10 Å was applied to retain 125−148 nearby water molecules, which were treated at the MM level using SPC and SPCpol potentials (the latter accounts for explicit solvent polarization effects), while the acetone molecule was treated quantum mechanically by the CCSD/aug-cc-pVDZ method.[28] In our computation of the vertical n→π* excitation energy of acetone in water using solute−solvent clusters, we include a much smaller number of water molecules explicitly (up to 12 water molecules) because we treat them quantum mechanically (rather than by molecular mechanics), and we treat the rest within the continuum approximation (cLR/PCM), which Aidas et al.[28] did not use. In additional calculations, Aidas et al. treated two explicit water molecules quantum mechanically by the CCSD/aug-cc-pVDZ method with no implicit solvent.[28]

Chipman[75] calculated the vertical n→π* excitation energy of acetone in water using an extension of the SVPE and SS(V)PE solvation models to treat the nonequilibrium solvation effects. The SVPE and SS(V)PE results were compared to those obtained using the conductor-like and dielectric versions of PCM, respectively, C-PCM and D-PCM. The author discussed the quantum mechanical computation of vertical transitions in solution in regard to volume polarization effects arising from penetration of the solute charge density outside the cavity.[75] The sensitivity of the computed vertical energies to the cavity size was noted.[75]

4. Summary

The inclusion of solvent effects beyond bulk electrostatics, for example, cavitation and dispersion, has been shown to be a key ingredient in calculating accurate free energies of solvation for equilibrated solutes in their ground electronic states.[88,89,115,116] A related challenge is the inclusion of these same effects in the treatment of condensed-phase electronic excitation. In this work, we computed the vertical n→π* electronic excitation energy of acetone in 22 nonaqueous solvents and in water including the contributions of (i) nonequilibrium electrostatic polarization, (ii) changes in solvent−solute dispersion, (iii) changes in solvent−solute hydrogen-bonding, and (iv) ground-state geometry relaxation. The solvatochromic shifts ($\Delta\omega$) on the vertical electronic excitation energies relative to the gas phase were computed

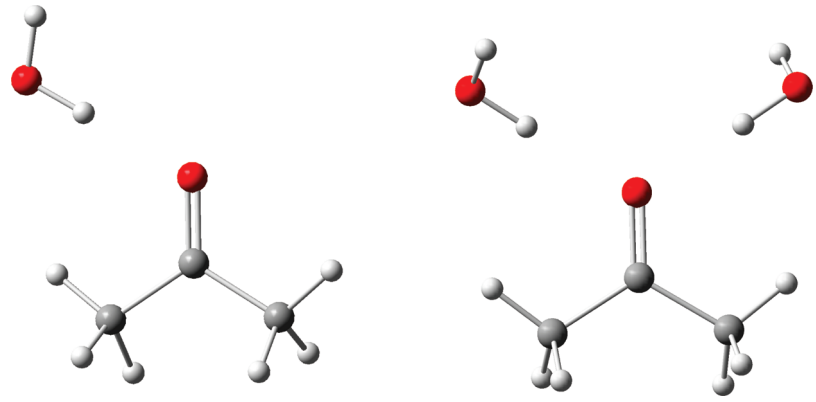

Figure 2. Molecular structures of the solute−solvent clusters containing one and two explicit water molecules optimized in solution at the SMD/M06-2X/MG3S level of theory. See caption to Figure 1 for atom colors.

Table 10. Recent Computations on the Vertical n→π* Excitation Energies (ω, cm^{-1}) of Acetone in Water

method	reference	ω(gas)	ω(water)	$\Delta\omega$
PCM/CASSCF/6-31G(d)[a,b]	Cossi and Barone[21]	37 195	37 964	−769
PCM/CASSCF/6-31G(d)/cluster[a,c,d]	Cossi and Barone[21]	37 195	39 592	−2397
PCM/TD-PBE0/6-311++G(2d,2p)[b]	Aquilante et al.[22]	35 730	36 779	−1049
PCM/TD-PBE0/6-311++G(2d,2p)/cluster[c]	Aquilante et al.[22]	35 730	38 795	−3065
PCM/TD-PBE0/6-311++G(2d,2p)/cluster[c,e]	Aquilante et al.[22]	35 730	37 263	−1533
CCSD/aug-cc-pVDZ/cluster[f]	Aidas et al.[28]	36 698	38 279	−1581
QM/MM(SPCpol) CCSD/aug-cc-pVDZ[g]	Aidas et al.[28]	36 698	37 795	−1097
SS(V)PE/CASSCF/6-311(2+)G(d)[h]	Chipman[75]	36 618	37 910	−1292
SS(V)PE/CASSCF/6-311(2+)G(d)[i]	Chipman[75]	36 618	38 876	−2258
cLR/PCM/TD-M06[b,j]	present	36 067	37 576	−1509
cLR/PCM/TD-M06/cluster[k]	present	36 067	37 742	−1675
experiment[l]	Bayliss et al.[6]	36 100	37 800	−1700
experiment[l]	Renge[9]	35 975	37 760	−1785 ± 7

[a] With nonequilibrium electrostatics and quantum-mechanical dispersion−repulsion contributions. [b] No explicit water molecules. [c] With two explicit water molecules. [d] Using a cluster called "Conformation 1" in ref 21. [e] Averaged over 40 acetone−water clusters (see ref 22 for more detail). [f] Linear response coupled cluster theory with two explicit water molecules added and with no implicit solvent. [g] The combined linear response coupled cluster/molecular mechanics (CC/MM) scheme including mutual polarization effects; the acetone molecule was treated at the CCSD/aug-cc-pVDZ level, whereas at most 148 explicit water molecules were treated at the MM level. [h] With the cavity size defined by solute electronic isodensity contours of ρ_o = 0.0005 au. [i] With the cavity size defined by solute electronic isodensity contours of ρ_o = 0.002 au. [j] See Table 3. [k] Averaged over 20 acetone−water clusters containing 12 explicit water molecules treated as part of a quantum mechanical supermolecule (Table 9). [l] UV absorption.

using two different continuum solvation models for calculating the electrostatic component of the shifts. One of the electrostatic models is based on the generalized Born approximation, and another solves the nonhomogeneous Poisson equation for electrostatics in terms of the integral-equation-formalism polarizable continuum model. Both models use a two-response-time electrostatic reaction field corresponding to equilibrated fast (electronic) solvent response and nonequilibrated Franck−Condon-defined slow (nuclear) solvent response. The dependence of calculated solvatochromic shifts on the values of the intrinsic atomic Coulomb radii used for construction of the boundary between the solute cavity and the solvent continuum in the bulk electrostatic calculations was investigated.

In addition to studies using a fully continuum representation of water, we also examined the effect of adding up to 12 explicit water molecules for the calculation of $\Delta\omega$ for acetone in aqueous solution. Sets of 20 random acetone−water configurations were taken from molecular dynamics trajectories, and in each case solvatochromic shifts were computed for the cluster of solute and explicit solvent molecules surrounded by a continuum representing the rest of the aqueous solvent.

On the basis of the results of these calculations, we draw five key conclusions:

(1) Although nonbulk-electrostatic contributions to solvatochromic shifts are usually neglected in modern calculations, they are not necessarily small in magnitude. In particular, we find that reasonable choices of cavity radii lead to dispersion contributions to the solvatochromism of acetone on the order of 300−400 cm^{-1} in all solvents.

(2) Hydrogen-bonding contributions were even larger in magnitude than dispersion effects in solvents having strong hydrogen-bond-donating ability. When the electrostatic cavity is constructed from oxygen radii that are large in water and independent of solvent (e.g., scaled UFF radii), explicit corrections for hydrogen bonding must be made to improve predictive accuracy. Some SMD radii, including oxygen radii, by contrast depend on the solvent hydrogen-bond donating character, and as a result additional corrections for the effect of changes in hydrogen bonding on acetone solvatochromism were up to an order of magnitude smaller.

(3) When nonbulk-electrostatic contributions are explicitly included in the solvation model, they can ameliorate unphysical choices for the atomic radii used in the construction of the solute cavity in the purely continuum electrostatics

calculation. Nevertheless, analysis of trends in the magnitudes (and signs) of the correction terms renders clear which sets of radii should be regarded as most physically appropriate. From such an analysis, we conclude that SMD radii, which were optimized for the computation of ground-state free energies of solvation and not previously examined for the prediction of solvatochromism, represent the optimal available combination of accuracy and physicality. The use of UFF radii scaled by a factor of 1.1 also gave good results for the quantitative prediction of solvatochromic shifts, but only after the addition of a substantially larger correction for changes in hydrogen bonding than was needed for SMD. As noted above, this reflects the ability of the SMD model to capture such effects through the use of solvent-dependent atomic cavity radii. Insofar as post hoc corrections for changes in hydrogen bonding are not easily calculated (in the absence of a large set of solvatochromic training data), and moreover such corrections are not included in the relaxation of the excited-state wave function (which may lead to other computed properties being inaccurate), we recommend the use of SMD radii in place of scaled UFF radii. We note that this conclusion is based on the limited data in the present Article, and its generality needs to be investigated beyond carbonyl compounds, but the calculations presented here indicate that significant quantitative errors can be obtained if solvatochromic shifts are calculated with scaled or unscaled molecular mechanics radii *and only the influence of bulk electrostatics is considered*.

(4) The optimization of acetone−water clusters including a small number of water molecules does not lead to substantially improved predictions for the aqueous solvatochromic shift when these clusters are embedded in the continuum. It appears that the water−acetone hydrogen-bonding interactions in the optimized cluster are too strong as compared to those that would be found in bulk solution. Indeed, when clusters are not optimized but instead removed from molecular dynamics trajectories in explicit water, the influence of bulk water molecules on the first solvation shell around acetone manifests itself in smaller predicted blue shifts that are in much better agreement with experiment. Predicted shifts from the extracted-cluster protocol converge very quickly with the number of water molecules n chosen to be explicitly retained. With SMD radii, results for $n = 2$, 5, 8, 10, and 12 are within one standard deviation of one another when averaged over 20 snapshots. For $n = 12$, $\Delta\omega = -1675$ cm^{-1} calculated with the M06 density functional approximation agrees well with the experimental[9] $\Delta\omega = -1785$ cm^{-1}. The use of UFF radii scaled by a factor of 1.1 for the same clusters leads to an underestimated blue shift, $\Delta\omega = -1146$ cm^{-1}. As the acetone carbonyl oxygen is effectively buried by the explicit solvent shell, this suggests that the improved performance of the SMD radii is associated not only with the acetone molecule, but also the surrounding water molecules. We conclude that treating only a few water molecules explicitly with structures optimized for the cluster (supersolute) (rather than averaging over a canonical ensemble of structures selected from a simulation of the bulk) leads to significant systematic errors.

(5) Because the standard deviation of the solvatochromic shift predicted from the molecular dynamics trajectory snapshots measures the broadening of the excited-state absorption due to thermal fluctuations in the surrounding medium, we were able to see that the width of the distribution of solvatochromic shifts in water is large. In particular, we calculate a standard deviation of 474 cm^{-1} of the single-molecule shifts from their mean. If one compares this to the predicted solvatochromic shift of -1675 cm^{-1}, one sees that the width of the distribution is not insignificant, and one should keep this heterogeneity in mind in interpreting solvatochromic shifts in general.

Finally, in addition to considering experimental results previously reported in the literature, we have also predicted the vertical n→π* electronic excitation energies of acetone in 160 nonaqueous solvents that were not included in the training set of 23 solvents[9] (see the Supporting Information). These predictions should prove interesting for comparison to future measurements.

Acknowledgment. We are grateful to Dr. Carlos P. Sosa (IBM and Minnesota Supercomputing Institute) for invaluable assistance. This work was supported by the Army Research Office under grant US ARMY RES LAB/W911NF09-1-0377 and by the National Science Foundation under grants CHE06-10183, CHE07-04974, and CHE09-56776.

Supporting Information Available: Vertical excitation energies and solvatochromic shifts for the n→π* transition of acetone in water calculated using acetone−water clusters and implicit solvent models; vertical excitation energies and solvatochromic shifts for the n→π* transition of acetone in water calculated using acetone−water clusters with one and two explicit water molecules; vertical excitation energies and solvatochromic shifts for the n→π* transition of acetone in the 178 nonaqueous solvents in the Minnesota Solvent Descriptor Database (the set of 23 solvents studied in the paper includes, in addition to water, 18 nonaqueous solvents that are among 178 solvents in that database and 4 nonaqueous solvents (perfluoro-*n*-octane, tetraethoxysilane, *tert*-butyl chloride, and propylene carbonate) that are not in the database); and Cartesian coordinates of the acetone molecule in the ground electronic state optimized in the gas phase and in solution. This material is available free of charge via the Internet at http://pubs.acs.org.

References

(1) Bayliss, N. S.; McRae, E. G. *J. Phys. Chem.* **1954**, *58*, 1006.

(2) Pimentel, G. C. *J. Am. Chem. Soc.* **1957**, *79*, 3323.

(3) Ito, M.; Inuzuka, K.; Imanishi, S. *J. Am. Chem. Soc.* **1960**, *82*, 1317.

(4) Balasubramanian, A.; Rao, C. N. R. *Spectrochim. Acta* **1962**, *18*, 1337.

(5) Hayes, W. P.; Timmons, C. J. *Spectrochim. Acta* **1965**, *21*, 529.

(6) Bayliss, N. S.; Wills-Johnson, G. *Spectrochim. Acta* **1968**, *24A*, 551.

(7) Yudasaka, M.; Hosoya, H. *Bull. Chem. Soc. Jpn.* **1978**, *51*, 1708.

(8) Xu, H.; Wentworth, P. J.; Howell, N. W.; Joens, J. A. *Spectrochim. Acta* **1993**, *49A*, 1171.

(9) Renge, I. *J. Phys. Chem. A* **2009**, *113*, 10678.

(10) Fox, T.; Rösch, N. *Chem. Phys. Lett.* **1992**, *191*, 33.

(11) Pappalardo, R. R.; Reguero, M.; Robb, M. A.; Frisch, M. *Chem. Phys. Lett.* **1993**, *212*, 12.

(12) Rösch, N.; Zerner, M. C. *J. Phys. Chem.* **1994**, *98*, 5817.

(13) Ten-no, S.; Hirata, F.; Kato, S. *J. Chem. Phys.* **1994**, *100*, 7443.

(14) Gao, J. *J. Am. Chem. Soc.* **1994**, *116*, 9324.

(15) Liao, D. W.; Mebel, A. M.; Chen, Y.-T.; Lin, S.-H. *J. Phys. Chem. A* **1997**, *101*, 9925.

(16) Serrano-Andrés, L.; Fülscher, M. P.; Karlström, G. *Int. J. Quantum Chem.* **1997**, *65*, 167.

(17) Mennucci, B.; Cammi, R.; Tomasi, J. *J. Chem. Phys.* **1998**, *109*, 2798.

(18) Coutinho, K.; Saavedra, N.; Canuto, S. *THEOCHEM* **1999**, *466*, 69.

(19) Li, J.; Cramer, C. J.; Truhlar, D. G. *Int. J. Quantum Chem.* **2000**, *77*, 264.

(20) Martin, M. E.; Sanchez, M. L.; Olivares del Valde, F. J.; Aguilar, M. A. *J. Chem. Phys.* **2000**, *113*, 6308.

(21) Cossi, M.; Barone, V. *J. Chem. Phys.* **2000**, *112*, 2427.

(22) Aquilante, F.; Cossi, M.; Crescenzi, O.; Scalmani, G.; Barone, V. *Mol. Phys.* **2003**, *101*, 1945.

(23) Röhrig, U. F.; Frank, I.; Hutter, J.; Laio, A.; VandeVondele, J.; Rothlisberger, U. *ChemPhysChem* **2003**, *4*, 1177.

(24) Bernasconi, L.; Sprik, M.; Hutter, J. *J. Chem. Phys.* **2003**, *119*, 12417.

(25) Coutinho, K.; Canuto, S. *THEOCHEM* **2003**, *632*, 235.

(26) Crescenzi, O.; Pavone, M.; De Angelis, F.; Barone, V. *J. Phys. Chem. B* **2005**, *109*, 445.

(27) Sulpizi, M.; Röhrig, U. F.; Hutter, J.; Rothlisberger, U. *Int. J. Quantum Chem.* **2005**, *101*, 671.

(28) Aidas, K.; Kongsted, J.; Osted, A.; Mikkelsen, K. V.; Christiansen, O. *J. Phys. Chem. A* **2005**, *109*, 8001.

(29) Öhrn, A.; Karlström, G. *Theor. Chem. Acc.* **2007**, *117*, 441.

(30) Fonseca, T. L.; Coutinho, K.; Canuto, S. *J. Chem. Phys.* **2007**, *126*, 034508.

(31) Minezawa, N.; Kato, S. *J. Chem. Phys.* **2007**, *126*, 054511.

(32) Lin, Y.-l.; Gao, J. *J. Chem. Theory Comput.* **2007**, *3*, 1484.

(33) Gomes, A. S. P.; Jacob, C. R.; Visscher, L. *Phys. Chem. Chem. Phys.* **2008**, *10*, 5353.

(34) Liptay, W. *Z. Naturforsch.* **1965**, *20A*, 1441.

(35) Aguilar, M. A.; Olivares del Valle, F. J.; Tomasi, J. *J. Chem. Phys.* **1993**, *98*, 7375.

(36) Ridley, J. E.; Zerner, M. C. *Theor. Chim. Acta* **1973**, *32*, 111.

(37) Zerner, M. C. *Rev. Comput. Chem.* **1991**, *2*, 313.

(38) Li, J.; Williams, B.; Cramer, C. J.; Truhlar, D. G. *J. Chem. Phys.* **1999**, *110*, 724.

(39) Zerner, M. C.; Ridley, J. E.; Bacon, A. D.; Edwards, W. D.; Head, J. D.; McKelvey, J.; Culberson, J. C.; Knappe, P.; Cory, M. G.; Weiner, B.; Baker, J. D.; Parkinson, W. A.; Kannis, D.; Yu, J.; Roesch, N.; Kotzian, M.; Tamm, T.; Karelson, M. M.; Zheng, X.; Pearl, G.; Broo, A.; Albert, K.; Cullen, J. M.; Cramer, C. J.; Truhlar, D. G.; Li, J.; Hawkins, G. D.; Liotard, D. A. *ZINDO computer program - version 99.1*, 1999.

(40) Cossi, M.; Barone, V. *J. Chem. Phys.* **2001**, *115*, 4708.

(41) Runge, E.; Gross, E. K. U. *Phys. Rev. Lett.* **1984**, *52*, 997.

(42) Casida, M. E. In *Time-Dependent Density-Functional Response Theory for Molecules*; Chong, D. P., Ed.; World Scientific: Singapore, 1995; Vol. 1, p 155.

(43) Bauernschmitt, R.; Ahlrichs, R. *Chem. Phys. Lett.* **1996**, *256*, 454.

(44) Stratmann, R. E.; Scuseria, G. E.; Frisch, M. J. *J. Chem. Phys.* **1998**, *109*, 8218.

(45) Tomasi, J.; Persico, M. *Chem. Rev.* **1994**, *94*, 2027.

(46) Cramer, C. J.; Truhlar, D. G. *Chem. Rev.* **1999**, *99*, 2161.

(47) Cramer, C. J.; Truhlar, D. G. In *Free Energy Calculations in Rational Drug Design*; Reddy, M. R., Erion, M. D., Eds.; Kluwer Academic/Plenum: New York, 2001; p 63.

(48) Tomasi, J.; Mennucci, B.; Cammi, R. *Chem. Rev.* **2005**, *105*, 2999.

(49) Mennucci, B. In *Continuum Solvation Models in Chemical Physics*; Mennucci, B., Cammi, R., Eds.; Wiley: Chichester, U.K., 2007; p 110.

(50) Marcus, R. A. *J. Chem. Phys.* **1956**, *24*, 966.

(51) Aguilar, M. A. *J. Phys. Chem. A* **2001**, *105*, 10393.

(52) Marcus, R. A. *J. Chem. Phys.* **1956**, *24*, 979.

(53) Wolynes, P. G. *J. Chem. Phys.* **1987**, *86*, 5133.

(54) Hsu, C.-P.; Song, X.; Marcus, R. A. *J. Phys. Chem. B* **1997**, *101*, 2546.

(55) Basilevsky, M. V.; Parsons, D. F.; Vener, M. V. *J. Chem. Phys.* **1998**, *108*, 1103.

(56) Caricato, M.; Ingrosso, F.; Mennucci, B.; Tomasi, J. *J. Chem. Phys.* **2005**, *122*, 154501.

(57) Hoijtink, G. J.; de Boer, E.; van der Meij, P. H.; Weijland, W. P. *Recl. Trav. Chim. Pays-Bas Belg.* **1956**, *75*, 487.

(58) Peradejordi, F. *Cahiers Phys.* **1963**, *17*, 393.

(59) Klopman, G. *Chem. Phys. Lett.* **1967**, *1*, 200.

(60) Tapia, O. In *Quantum Theory of Chemical Reactions*; Daudel, R., Pullman, A., Salem, L., Viellard, A., Eds.; Wiley: London, 1981; Vol. 2, p 25.

(61) Tucker, S. C.; Truhlar, D. G. *Chem. Phys. Lett.* **1989**, *157*, 164.

(62) Still, W. C.; Tempczyk, A.; Hawley, R. C.; Hendrickson, T. *J. Am. Chem. Soc.* **1990**, *112*, 6127.

(63) Mikkelsen, K. V.; Cesar, A.; Ågren, H.; Jensen, H. J. Aa. *J. Chem. Phys.* **1995**, *103*, 9010.

(64) Miertuś, S.; Scrocco, E.; Tomasi, J. *Chem. Phys.* **1981**, *55*, 117.

(65) Miertuś, S.; Tomasi, J. *Chem. Phys.* **1982**, *65*, 239.

(66) Improta, R.; Barone, V.; Scalmani, G.; Frisch, M. J. *J. Chem. Phys.* **2006**, *125*, 054103.

(67) Improta, R.; Scalmani, G.; Frisch, M. J.; Barone, V. *J. Chem. Phys.* **2007**, *127*, 074504.

(68) Scalmani, G.; Frisch, M. J.; Mennucci, B.; Tomasi, J.; Cammi, R.; Barone, V. *J. Chem. Phys.* **2006**, *124*, 094107.

(69) Caricato, M.; Mennucci, B.; Tomasi, J.; Ingrosso, F.; Cammi, R.; Corni, S.; Scalmani, G. *J. Chem. Phys.* **2006**, *124*, 124520.

(70) Cancès, E.; Mennucci, B.; Tomasi, J. *J. Chem. Phys.* **1997**, *107*, 3032.

(71) Mennucci, B.; Tomasi, J. *J. Chem. Phys.* **1997**, *106*, 5151.

(72) Mennucci, B.; Cancès, E.; Tomasi, J. *J. Phys. Chem. B* **1997**, *101*, 10506.

(73) Tomasi, J.; Mennucci, B.; Cancès, E. *J. Mol. Struct. (THEOCHEM)* **1999**, *464*, 211.

(74) Chipman, D. M. *J. Chem. Phys.* **2009**, *131*, 014103.

(75) Chipman, D. M. *J. Chem. Phys.* **2009**, *131*, 014104.

(76) Zhan, C.-G.; Bentley, J.; Chipman, D. M. *J. Chem. Phys.* **1998**, *108*, 177.

(77) Chipman, D. M. *Theor. Chem. Acc.* **2002**, *107*, 80.

(78) Cancès, E.; Mennucci, B. *J. Chem. Phys.* **2001**, *114*, 4744.

(79) Cammi, R.; Corni, S.; Mennucci, B.; Tomasi, J. *J. Chem. Phys.* **2005**, *122*, 104513.

(80) Corni, S.; Cammi, R.; Mennucci, B.; Tomasi, J. *J. Chem. Phys.* **2005**, *123*, 134512.

(81) Li, J.; Zhu, T.; Cramer, C. J.; Truhlar, D. G. *J. Phys. Chem. A* **2000**, *104*, 2178.

(82) Pekar, S. I. *Untersuchungen über die Elektronentheorie der Kristalle*; Akademie-Verlag: Berlin, Germany, 1954.

(83) Cramer, C. J.; Truhlar, D. G. In *Solvent Effects and Chemical Reactivity*; Tapia, O., Bertran, J., Eds.; Understanding Chemical Reactivity Series; Kluwer: Dordrecht, The Netherlands, 1996; Vol. 17, p 1.

(84) Zhu, T.; Li, J.; Hawkins, G. D.; Cramer, C. J.; Truhlar, D. G. *J. Chem. Phys.* **1998**, *109*, 9117. errata: **1999**, *111*, 5624 and **2000**, *113*, 3930.

(85) Li, J.; Hawkins, G. D.; Cramer, C. J.; Truhlar, D. G. *Chem. Phys. Lett.* **1998**, *288*, 293.

(86) Li, J.; Zhu, T.; Hawkins, G. D.; Winget, P.; Liotard, D. A.; Cramer, C. J.; Truhlar, D. G. *Theor. Chem. Acc.* **1999**, *103*, 9.

(87) Cramer, C. J.; Truhlar, D. G. In *Trends and Perspectives in Modern Computational Science*; Maroulis, G., Simos, T. E., Eds.; Lecture Series on Computer and Computational Sciences 6; Brill/VSP: Leiden, The Netherlands, 2006; p 112.

(88) Cramer, C. J.; Truhlar, D. G. *Acc. Chem. Res.* **2008**, *41*, 760.

(89) Cramer, C. J.; Truhlar, D. G. *Acc. Chem. Res.* **2009**, *42*, 493.

(90) Li, J.; Zhu, T.; Cramer, C. J.; Truhlar, D. G. *J. Phys. Chem. A* **1998**, *102*, 1820.

(91) Zerner, M. C.; Ridley, J. E.; Bacon, A. D.; Edwards, W. D.; Head, J. D.; McKelvey, J.; Culberson, J. C.; Knappe, P.; Cory, M. G.; Weiner, B.; Baker, J. D.; Parkinson, W. A.; Kannis, D.; Yu, J.; Roesch, N.; Kotzian, M.; Tamm, T.; Karelson, M. M.; Zheng, X.; Pearl, G.; Broo, A.; Albert, K.; Cullen, J. M.; Li, J.; Hawkins, G. D.; Thompson, J. D.; Kelly, C. P.; Liotard, D. A.; Cramer, C. J.; Truhlar, D. G. *ZINDO-MN1.2, Quantum Theory Project*; University of Florida, Gainesville, and Department of Chemistry, University of Minnesota, Minneapolis, 2005.

(92) Lynch, B. J.; Zhao, Y.; Truhlar, D. G. *J. Phys. Chem. A* **2003**, *107*, 1384.

(93) Frisch, M. J.; Trucks, G. W.; Schlegel, H. B.; Scuseria, G. E.; Robb, M. A.; Cheeseman, J. R.; Scalmani, G.; Barone, V.; Mennucci, B.; Petersson, G. A.; Nakatsuji, H.; Caricato, M.; Li, X.; Hratchian, H. P.; Izmaylov, A. F.; Bloino, J.; Zheng, G.; Sonnenberg, J. L.; Hada, M.; Ehara, M.; Toyota, K.; Fukuda, R.; Hasegawa, J.; Ishida, M.; Nakajima, T.; Honda, Y.; Kitao, O.; Nakai, H.; Vreven, T.; Montgomery, J. A., Jr.; Peralta, J. E.; Ogliaro, F.; Bearpark, M.; Heyd, J. J.; Brothers, E.; Kudin, K. N.; Staroverov, V. N.; Kobayashi, R.; Normand, J.; Raghavachari, K.; Rendell, A.; Burant, J. C.; Iyengar, S. S.; Tomasi, J.; Cossi, M.; Rega, N.; Millam, N. J.; Klene, M.; Knox, J. E.; Cross, J. B.; Bakken, V.; Adamo, C.; Jaramillo, J.; Gomperts, R.; Stratmann, R. E.; Yazyev, O.; Austin, A. J.; Cammi, R.; Pomelli, C.; Ochterski, J. W.; Martin, R. L.; Morokuma, K.; Zakrzewski, V. G.; Voth, G. A.; Salvador, P.; Dannenberg, J. J.; Dapprich, S.; Daniels, A. D.; Farkas, Ö.; Foresman, J. B.; Ortiz, J. V.; Cioslowski, J.; Fox, D. J. *Gaussian 09*, revision A.02; Gaussian, Inc.: Wallingford, CT, 2009.

(94) *Gaussian09 User's Reference: SCRF*; http://www.gaussian.com/g-tech/g_ur/k_scrf.htm (accessed May 19, 2010).

(95) Marenich, A. V.; Cramer, C. J.; Truhlar, D. G. *J. Phys. Chem. B* **2009**, *113*, 6378.

(96) Zhao, Y.; Truhlar, D. G. *Theor. Chem. Acc.* **2008**, *120*, 215.

(97) Zhao, Y.; Truhlar, D. G. *Acc. Chem. Res.* **2008**, *41*, 157.

(98) Reichardt, C. *Solvents and Solvent Effects in Organic Chemistry*, 2nd ed.; VCH: Weinheim, 1990; Chapter 6.

(99) Abraham, M. H.; Grellier, P. L.; Prior, D. V.; Duce, P. P.; Morris, J. J.; Taylor, P. J. *J. Chem. Soc., Perkin Trans. 2* **1989**, 699.

(100) Abraham, M. H. *Chem. Soc. Rev.* **1993**, *22*, 73.

(101) Abraham, M. H. *J. Phys. Org. Chem.* **1993**, *6*, 660.

(102) Abraham, M. H. In *Quantitative Treatment of Solute/Solvent Interactions; Theoretical and Computational Chemistry Series Vol. 1*; Politzer, P., Murray, J. S., Eds.; Elsevier: Amsterdam, 1994; p 83.

(103) Winget, P.; Dolney, D. M.; Giesen, D. J.; Cramer, C. J.; Truhlar, D. G. *Minnesota Solvent Descriptor Database version 1999*; University of Minnesota: Minneapolis, MN, 1999; http://comp.chem.umn.edu/solvation/mnsddb.pdf (accessed March 18, 2010).

(104) Becke, A. D. *Phys. Rev. A* **1988**, *38*, 3098.

(105) Lee, C.; Yang, W.; Parr, R. G. *Phys. Rev. B* **1988**, *37*, 785.

(106) Becke, A. D. *J. Chem. Phys.* **1993**, *98*, 5648.

(107) Stephens, P. J.; Devlin, F. J.; Chabalowski, C. F.; Frisch, M. J. *J. Phys. Chem.* **1994**, *98*, 11623.

(108) Zhao, Y.; Truhlar, D. G. *J. Phys. Chem. A* **2006**, *110*, 13126.

(109) Zhao, Y.; Truhlar, D. G. *J. Chem. Phys.* **2006**, *125*, 194101.

(110) Foresman, J. B.; Head-Gordon, M.; Pople, J. A.; Frisch, M. J. *J. Phys. Chem.* **1992**, *96*, 135.

(111) Bondi, A. *J. Phys. Chem.* **1964**, *68*, 441.

(112) Barone, V.; Improta, R.; Rega, N. *Theor. Chem. Acc.* **2004**, *111*, 237.

(113) Barone, V.; Cossi, M.; Tomasi, J. *J. Chem. Phys.* **1997**, *107*, 3210.

(114) Rappé, A. K.; Casewit, C. J.; Colwell, K. S.; Goddard, W. A., III; Skiff, W. M. *J. Am. Chem. Soc.* **1992**, *114*, 10024.

(115) Curutchet, C.; Cramer, C. J.; Truhlar, D. G.; Ruiz-López, M. F.; Rinaldi, D.; Orozco, M.; Luque, F. J. *J. Comput. Chem.* **2003**, *24*, 284.

(116) Marenich, A. V.; Cramer, C. J.; Truhlar, D. G. *J. Chem. Theory Comput.* **2008**, *4*, 877.

(117) Jacquemin, D.; Perpète, E. A.; Ciofini, I.; Adamo, C.; Valero, R.; Zhao, Y.; Truhlar, D. G. *J. Chem. Theory Comput.* **2010**, *6*, 2071.

(118) Singh, U. C.; Kollman, P. A. *J. Comput. Chem.* **1984**, *5*, 129.

(119) Besler, B. H.; Merz, K. M., Jr.; Kollman, P. A. *J. Comput. Chem.* **1990**, *11*, 431.

(120) *CRC Handbook of Chemistry and Physics*; Lide, D. R., Ed.; Taylor and Francis: Boca Raton, FL, 2010; Vol. 90 (Internet Version 2010, http://www.hbcpnetbase.com).

(121) *MacroModel, version 9.6*; Schrödinger, LLC: New York, 2008.

(122) *Maestro Version 8.5.111, MMshare Version 1.7.110*; Schrödinger, LLC: New York, 2008.

(123) Banks, J. L.; Beard, H. S.; Cao, Y.; Cho, A. E.; Damm, W.; Farid, R.; Felts, A. K.; Halgren, T. A.; Mainz, D. T.; Maple, J. R.; Murphy, R.; Philipp, D. M.; Repasky, M. P.; Zhang, L. Y.; Berne, B. J.; Friesner, R. A.; Gallicchio, E.; Levy, R. M. *J. Comput. Chem.* **2005**, *26*, 1752.

(124) Jorgensen, W. L.; Maxwell, D. S.; Tirado-Rives, J. *J. Am. Chem. Soc.* **1996**, *118*, 11225.

CT100267S